Mechanical Limits of Fracture-Driven Pressure Relaxation in Diamond-Hosted Olivine Inclusions: Constraints from 3D Phase-Field and XFEM Modelling

Biswabhanu Puhan

Department of Earth and Environmental Sciences, University of Pavia, Via A. Ferrata 1, 27100 Pavia

DOI: 10.19276/plinius.2026.01.017

INTRODUCTION

Diamonds erupted in kimberlite pipes from the lithospheric and sub-lithospheric mantle carry within them some of the most direct physical records of deep-Earth conditions available to science. Mineral inclusions trapped during diamond growth preserve residual stresses that encode the pressure–temperature (*P*–*T*) state at the moment of encapsulation, providing a rare and irreplaceable window into environments otherwise inaccessible to direct sampling. In kimberlitic systems such as Udachnaya (Siberia), olivine inclusions are among the most abundant and analytically tractable of these natural gauges. Their residual stress state – measured with micro-Raman spectroscopy and single-crystal X-ray diffraction – combined with the contrasting elastic properties of host and inclusion, forms the basis of elastic geobarometry: the primary quantitative method for reconstructing diamond entrapment depths and inferring first-order geological quantities including lithospheric thickness, craton stability, mantle metasomatic history, and the deep carbon cycle (Pearson et al., 2014; Nestola et al., 2018; Angel et al., 2022; Kohn et al., 2023).

The central assumption of elastic geobarometry is that both host and inclusion behave as purely elastic solids throughout exhumation. Under this assumption, the thermoelastic mismatch between diamond – significantly stiffer and with lower thermal expansivity than olivine – generates a residual overpressure in the inclusion once surface conditions are reached. For representative entrapment conditions of 5.5 GPa and 1473 K – consistent with olivine inclusions from Udachnaya (Nestola et al., 2011; Agrosì et al., 2016) – coupling the equations of state of diamond and olivine yields a thermoelastic overpressure of approximately 1 GPa. Three-dimensional elastic simulations reduce this to a relaxed residual inclusion pressure of ~ 0.82 GPa, owing to geometric stress redistribution across the host–inclusion interface (Fig. 1).

Yet observations from Udachnaya and other kimberlitic localities systematically contradict this prediction. Olivine inclusions in natural diamonds routinely record residual pressures below 0.5 GPa (Rustioni et al., 2016; Angel et al., 2022) – values that, interpreted elastically, place entrapment conditions outside the diamond sta-

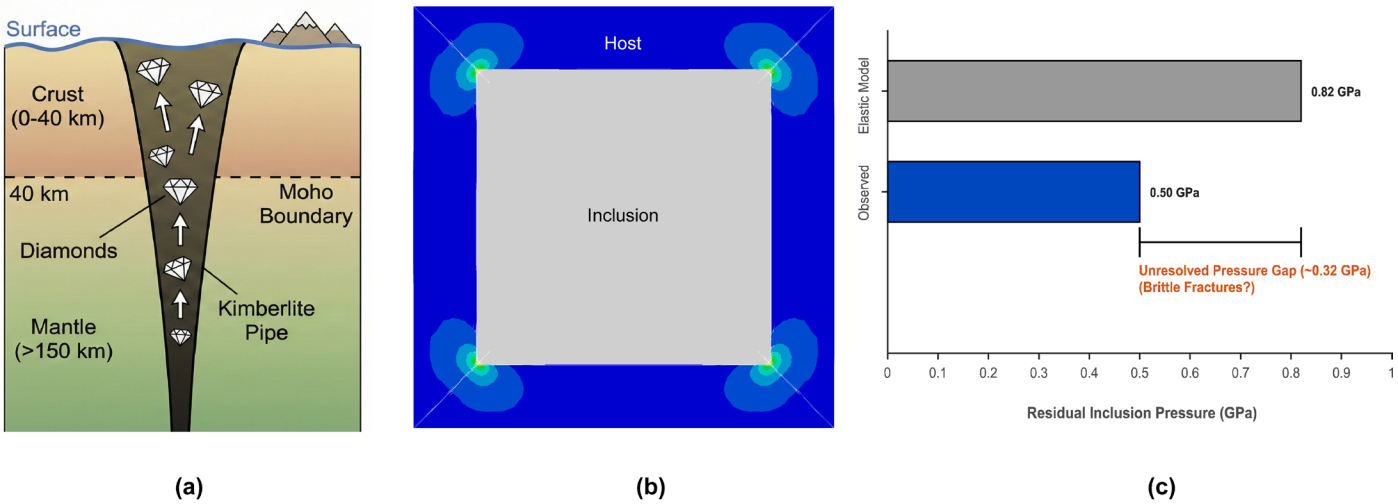

Figure 1 *Elastic stress distribution and residual pressure gap in diamond-hosted olivine inclusions.* ***a)*** *Geological schematic of kimberlitic ascent transporting diamonds from lithospheric mantle depths to the surface.* ***b)*** *Three-dimensional purely elastic simulation of a host–inclusion system illustrating stress concentration at geometric singularities resulting from thermoelastic mismatch during decompression.* ***c)*** *Comparison between residual pressures predicted by purely elastic geobarometric models (~ 0.82 GPa) and residual pressures measured in natural olivine inclusions from Udachnaya (~ 0.50 GPa). The persistent discrepancy (~ 0.32 GPa) defines the mechanical gap investigated in this thesis.*

bility field. This discrepancy of approximately 0.32 GPa defines a persistent mechanical gap (Fig. 1c). Several inelastic mechanisms have been proposed to account for it: time-dependent viscoplastic deformation of the diamond host, fluid-assisted weakening at host–inclusion boundaries, and brittle fracture (Nimis et al., 2016; Moulas et al., 2020; Campomenosi et al., 2023; Zhong et al., 2024). Among these, brittle fracture is the most directly observable – crack networks at host–inclusion boundaries are commonly documented in natural diamonds, frequently associated with thin silicic fluid films (Nimis et al., 2016). As the mechanically simplest and most observationally constrained candidate, brittle fracture must be rigorously evaluated first – and its limits quantified precisely – before more complex time-dependent mechanisms are invoked.

This thesis quantifies, for the first time through fully three-dimensional numerical modelling, the mechanical upper bound on pressure relaxation achievable through brittle and quasi-brittle fracture in diamond-hosted olivine inclusion systems. By systematically isolating the roles of inclusion geometry, edge sharpness, fracture strength, fracture toughness, inclusion volume, and multi-inclusion crack interaction, the work establishes a definitive mechanical benchmark against which natural observations can be evaluated.

METHODS, PROCEDURES, AND PROCESS

Thermoelastic prestress

Residual overpressure was calculated by coupling the equations of state (EoS) of diamond (Angel et al., 2015) and olivine (Angel et al., 2018) between representative entrapment conditions (5.5 GPa, 1473 K) and ambient surface conditions (0 GPa, 298 K), yielding Pthermo ≈ 1 GPa. This is imposed as a uniform hydrostatic prestress on the inclusion cavity in all simulations – the maximum worst-case driving force for fracture. At depth, lithostatic confinement suppresses the net overpressure; only at the surface is the full mismatch realised. The rapid ascent of kimberlite magmas – effectively limiting viscous relaxation during transport (Zhong et al., 2018) – further justifies this loading assumption.

XFEM–CZM framework

The Extended Finite Element Method (XFEM), coupled with a cohesive zone model (CZM), was first applied to model discrete brittle fracture around ellipsoidal inclusions – idealised point-singularity geometries (Puhan et al., 2025). This framework, implemented in Abaqus/Standard, allows crack initiation and propagation along evolving paths without predefined crack geometry through enrichment functions and a cohesive-zone formulation. Inclusion volumes from 102 to 106 μm^3 were explored across systematic variations of fracture strength and toughness.

Phase-Field Cohesive Zone Model (PF-CZM)

The core numerical contribution is a fully three-dimensional PF-CZM that extends the XFEM framework to cuboidal inclusion geometries with edge singularities. This formulation represents fracture as a continuous damage process governed by a scalar phase-field variable ϕ (0 = intact, 1 = fully fractured), evolved through variational energy minimisation. The energy functional separates tensile and compressive strain energy components (Miehe et al., 2010); crack irreversibility is enforced through a history-field variable. Degradation and crack-density functions (Wu, 2017) link the damage variable to a physically meaningful traction–separation law calibrated through tensile strength ft, critical energy release rate Gc, and phase-field length scale l. Unlike XFEM, PF-CZM naturally accommodates crack branching, coalescence, and stress localisation driven by sharp geometric features. The coupled displacement–phase-field system was implemented in Abaqus/Standard via a custom User Element (UEL) written in Fortran, solved monolithically via a quasi-Newton (BFGS) scheme.

Geometric configurations

Both ellipsoidal and cuboidal inclusion geometries were modelled: ellipsoidal inclusions in the XFEM–CZM framework as idealised point-singularity benchmarks, and cuboidal inclusions in the PF-CZM framework to represent the angular morphologies common in natural diamonds (Whitney et al., 2000). Edge singularity

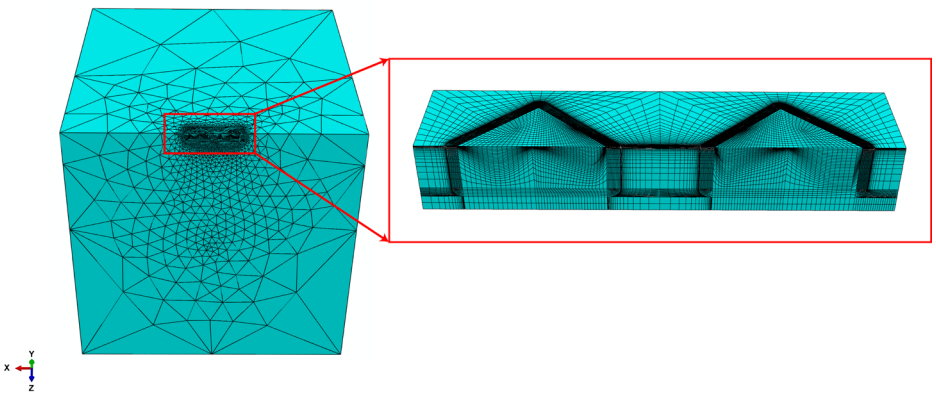

Figure 2 *Three-dimensional finite-element model of the two-inclusion configuration. Left: symmetry-reduced (1/4) host–inclusion domain used in simulations. Right: refined host region surrounding interacting cuboidal inclusions (spacing 57.6 μm), where phase-field fracture evolution is resolved. The hybrid mesh strategy ensures accurate stress-gradient capture near edge singularities while maintaining computational efficiency.*

sharpness was controlled parametrically via a fillet radius from 0.01 μm (near-ideal sharp edge) to 0.13 μm (blunted). Two cuboidal configurations were modelled: a symmetric four-edge inclusion (1/8th symmetry) and a single dominant-edge inclusion (1/4 symmetry). For multi-inclusion interaction studies, two single-edge cuboidal inclusions were embedded symmetrically at a separation of 57.6 μm – consistent with spacings documented in Udachnaya diamonds by X-ray tomography. The fracture zone was discretised with refined hexahedral elements transitioning to tetrahedral elements in the outer domain (Fig. 2).

RESULTS AND OBSERVATIONS

XFEM analysis: brittle fracture around ellipsoidal inclusions

XFEM–CZM simulations of ellipsoidal inclusions establish a first mechanical bound on brittle pressure relaxation (Puhan et al., 2025). Across the full range of inclusion volumes and fracture properties explored, purely brittle fracture reduces residual inclusion pressure from the elastic equilibrium of ~ 0.82 GPa to approximately 0.76 GPa – a reduction of only 5–6% of Pthermo. The critical fracture strength and toughness required for failure are approximately 0.738 GPa and ~ 1.4 MPa·m$^{0.5}$ respectively – values well below the lower experimental bounds for natural diamonds (Field & Pickles, 1996), confirming that fracture should occur under realistic conditions, yet delivers only marginal pressure relief. Even under these favourable conditions, residual pressures remain far above the < 0.5 GPa measured in Udachnaya olivines.

A robust scaling relation emerges: the critical fracture toughness for crack nucleation scales as the sixth root of inclusion volume ($K_{IC,crit} \propto V^{1/6}$), consistent with size-effect principles in fracture mechanics (Bažant, 2004), and persists across all geometric configurations explored – confirming it as a fundamental mechanical signature of the host–inclusion system. However, ellipsoidal models are an idealisation: natural olivine inclusions commonly exhibit angular morphologies with sharp edges and corners (Whitney et al., 2000), introducing edge singularities that may substantially alter fracture initiation and propagation. This motivates systematic investigation of cuboidal geometries using PF-CZM.

Geometry-controlled fracture: point singularities vs. edge singularities

The transition to cuboidal inclusion geometries reveals a two-stage fracture phenomenology absent in ellipsoidal models. Damage initiation ($0 < \phi < 1$) is governed exclusively by inclusion shape and host fracture strength, independently of inclusion volume and fracture toughness. For near-ideal sharp edges, a critical fracture strength of approximately 7.76 GPa is required to suppress damage initiation – consistent with the high-end experimental strength of single-crystal diamond.

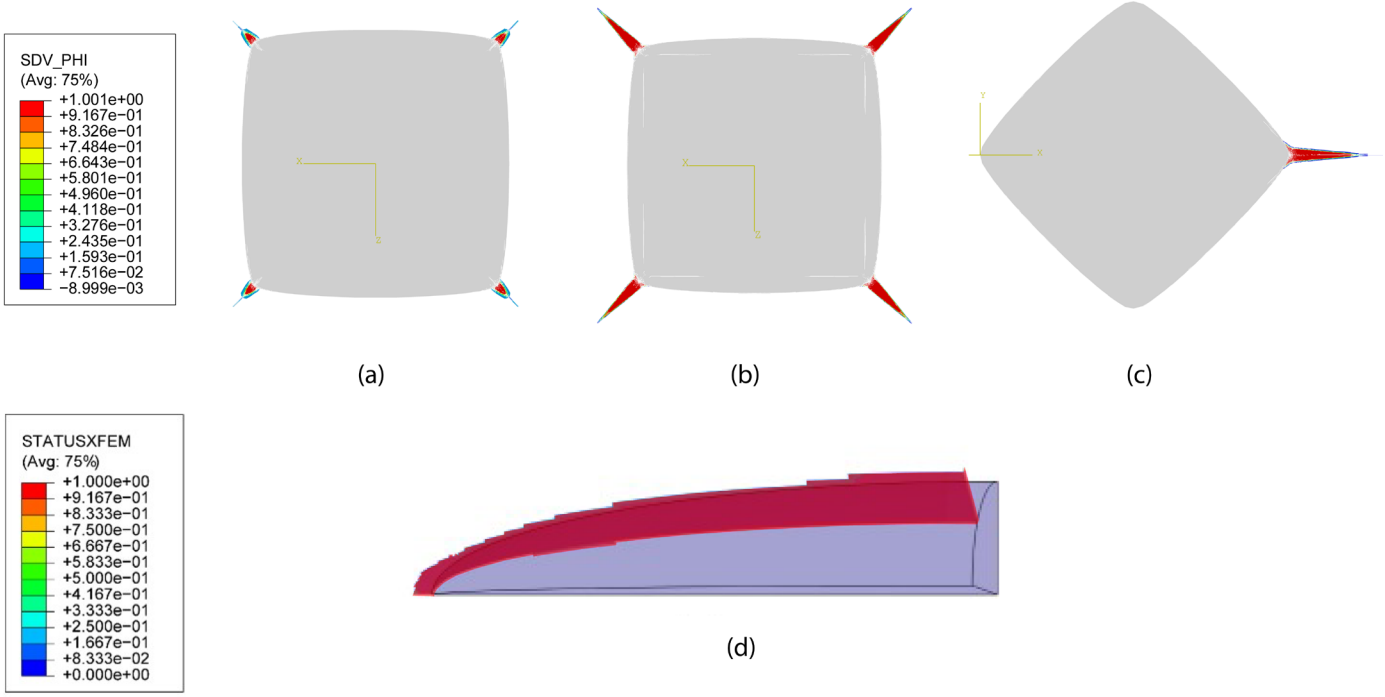

Figure 3 *Fracture patterns around cuboidal olivine inclusions with edge singularities (PF-CZM, panels a–c) and an ellipsoidal inclusion with point singularity (XFEM, panel d); all inclusions have a volume of 1 × 10^6 μm^3.* ***a)*** *Four-edge inclusion, comparative fracture strength (ft = 0.738 GPa).* ***b)*** *Four-edge inclusion, realistic fracture strength (ft = 3 GPa).* ***c)*** *Single-edge inclusion, comparative fracture strength (ft = 0.738 GPa). In panels (a–c), the phase-field variable ϕ is plotted: the white/grey diamond host is intact (ϕ = 0) and red regions are fully fractured (ϕ = 1); the white inclusion is shown in full, reconstructed by mirroring the symmetry-reduced domain.* ***d)*** *XFEM damage variable (STATUSXFEM) for fracture propagation around an ellipsoidal inclusion (aspect ratio 5:1:1, ft = 0.738 GPa): the blue body is the inclusion and red regions indicate fully fractured material; only 1/8th of the domain is shown consistent with the simulation symmetry. In both cases fracture is planar; however, cuboidal edge singularities drive fracture planes propagating outward away from the inclusion edges, whereas the ellipsoidal point singularity drives fracture planes propagating along the inclusion surface – inclusion geometry controls the direction of fracture propagation. Both independent numerical frameworks confirm that fracture alone cannot close the gap to natural residual pressures below 0.5 GPa.*

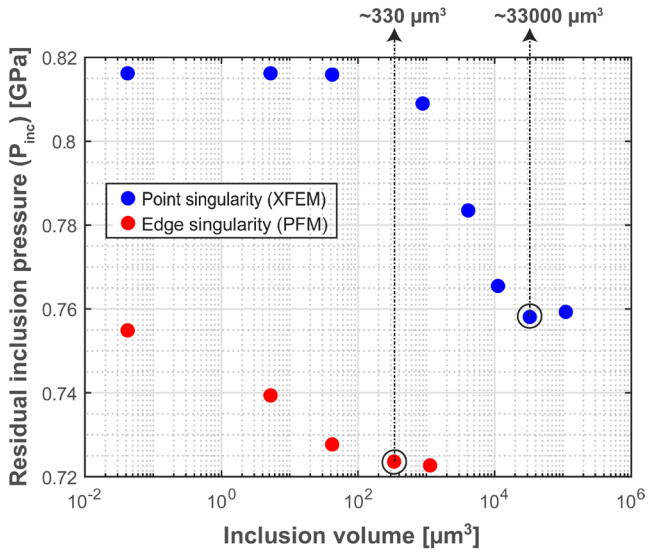

Figure 4 Comparison of residual inclusion pressure (Pinc) for point singularities (XFEM, blue) and edge singularities (PF-CZM, red) as a function of inclusion volume, under identical benchmark fracture parameters (ft = 0.738 GPa; KIC = 0.34 MPa·m^{0w5}). Edge singularities initiate and saturate fracture by ~330 μm³, while point singularities require volumes near ~ 33,000 μm³ to reach a similar plateau. Both geometries converge to stable residual pressures (~ 0.72 GPa and ~ 0.76 GPa, respectively) that remain well above the < 0.5 GPa measured in natural Udachnaya olivine inclusions, demonstrating that inclusion singularity type – not numerical framework – governs the onset and extent of stress relaxation, and that brittle fracture alone cannot reproduce natural observations.

As edges become progressively blunter, this threshold decreases to approximately 2.75 GPa. This geometry-dominated initiation regime has no equivalent in ellipsoidal models and demonstrates that angular inclusion morphologies, ubiquitous in natural diamonds, are substantially more fracture-prone than smooth ellipsoidal counterparts at equivalent material conditions. Figure. 3 illustrates this contrast directly: in cuboidal inclusions (PF-CZM) planar fractures propagate outward away from the inclusion edges, while in ellipsoidal inclusions (XFEM) planar fractures propagate along the inclusion surface – both are planar, but inclusion geometry controls the direction of fracture propagation.

Once fracture nucleation is achieved (ϕ = 1), inclusion volume and toughness jointly govern crack growth through the $V^{1/6}$ scaling law. As shown in Figure 4, edge singularities promote fracture initiation at inclusion volumes two orders of magnitude smaller than ellipsoidal geometries – saturation of residual pressure begins near ~ 330 μm³ for sharp cuboidal inclusions versus ~ 33,000 μm³ for point singularities. Despite this earlier initiation, the plateau residual pressure for cuboidal inclusions converges to ~ 0.72 GPa – only marginally lower than the ellipsoidal result of ~ 0.76 GPa. This is the central quantitative result: regardless of singularity type or numerical method, residual pressures plateau well above the < 0.5 GPa measured in natural Udachnaya olivines.

Additionally, cuboidal inclusions in the quasi-brittle regime – where diffuse damage accumulates (0 < ϕ < 1) without full crack nucleation – show progressive pressure reduction even in the absence of macroscopic fracture. This subcritical damage pathway provides partial relaxation at intermediate strength values, but does not alter the fundamental conclusion that the ~ 0.5 GPa natural threshold cannot be reached by any brittle or quasi-brittle mechanism.

Fracture nucleation landscape: strength, toughness, and size effects

A comprehensive fracture nucleation map in the strength–toughness parameter space (Fig. 5) reveals a non-monotonic, inverted-U-shaped boundary sep-

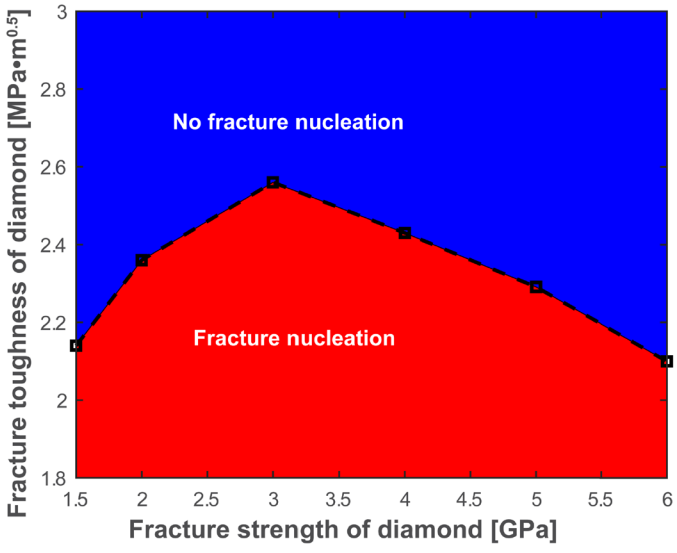

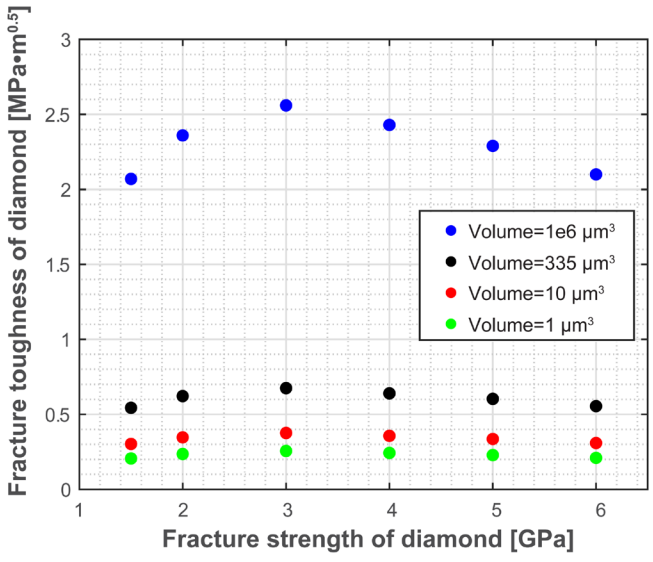

*Figure 5 Fracture nucleation map for an olivine inclusion in a diamond host. **a)** Critical fracture toughness required for crack nucleation as a function of fracture strength, for an inclusion volume of 1 × 10⁶ μm³. The red region indicates strength–toughness combinations where fracture nucleates; the blue region corresponds to stability (no fracture). The boundary follows a non-monotonic inverted-U shape: maximum fracture susceptibility occurs at intermediate strengths (~ 3 GPa). **b)** Nucleation boundaries for varying inclusion volumes. For large inclusions the inverted-U trend persists; as volume decreases, the system transitions to purely strength-controlled failure – consistent with size-effect principles in fracture mechanics (Bažant, 2004). The critical toughness scales as $V^{1/6}$ across all volumes, confirming the scaling law.*

arating stable (no fracture) from unstable (fracture nucleates) regimes. At intermediate fracture strengths (~ 3 GPa), the diamond host requires the highest fracture toughness to suppress crack nucleation – the condition of maximum fracture susceptibility. At both lower and higher strengths, the required toughness decreases: at low strength, diffuse microdamage initiates but insufficient elastic energy is available for coalescence into macroscopic cracks; at high strength, damage initiation is suppressed entirely. This behaviour is conceptually consistent with Ritchie's strength–toughness paradigm (Ritchie, 2011). The fracture nucleation boundary is volume-dependent: for small inclusions, the size effect suppresses toughness-controlled failure and the system becomes purely strength-controlled (Bažant, 2004). These results constitute the first comprehensive fracture nucleation diagram for diamond-hosted inclusion systems, spanning the complete natural variability of diamond mechanical properties.

Crack interaction and coalescence between neighbouring inclusions

Multiple olivine inclusions in natural Udachnaya diamonds are frequently found iso-oriented and chemically identical, suggesting they originated from a single grain – creating opportunities for fracture coalescence between neighbours (Angel et al., 2022). Two-inclusion PF-CZM simulations test whether crack interaction provides the additional relaxation that single-inclusion models cannot achieve. The results reveal that stress interaction substantially enhances fracture propagation – but delivers only limited additional pressure relaxation. Crack coalescence produces a continuous fracture pathway (Fig. 6), yet residual inclusion pressure does not fall below approximately 0.6 GPa. Fracture extent and pressure relaxation are mechanically decoupled: dramatic crack network growth does not translate proportionally into stress relief of the pressurised inclusion.

NOVEL CONTRIBUTIONS AND IMPLICATIONS

This thesis resolves a central and long-standing mechanical uncertainty at the core of elastic geobarometry: whether brittle fracture – the most visible and tractable inelastic mechanism in diamond–inclusion systems – can explain the anomalously low residual pressures documented in natural Udachnaya olivine inclusions.

The principal contribution is the establishment of the first mechanically rigorous, three-dimensional upper bound on fracture-driven pressure relaxation in these systems. The bound – approximately 0.72 GPa for cuboidal inclusions with edge singularities under realistic thermoelastic loading – is determined by systematic variation of all major controlling parameters: inclusion geometry, edge sharpness, fracture strength, toughness, volume, and inter-inclusion interaction. The remaining discrepancy of ~ 0.2–0.3 GPa between this bound and natural observations cannot be closed by any configuration of brittle or quasi-brittle fracture accessible within the physical parameter space of diamond–olivine systems. Additional inelastic mechanisms must therefore operate during ascent – most plausibly fluid-assisted weakening, where the silicic fluid films documented around Udachnaya olivine inclusions (Nimis et al., 2016) reduce effective fracture resistance, and/or time-dependent viscoplastic deformation of the diamond host at elevated temperatures during early stages of ascent.

These findings have direct consequences for elastic geobarometry worldwide. The implications extend beyond lithospheric diamonds: elastic geobarometry is applied equally to sub-lithospheric diamonds, which provide rare direct windows into otherwise inaccessible regions of the deep mantle (Pearson et al., 2014; Nestola et al., 2018). Furthermore, because fluid films at olivine–diamond interfaces in Udachnaya record rare earth element (REE) mobility and partitioning in kimberlitic systems (Weiss et al., 2022), erroneous residual pressure estimates propagate directly into geochemical interpretations of mantle metasomatism and the deep carbon cycle. Residual pressures below ~ 0.72 GPa in olivine inclusions cannot be attributed to fracture alone; they require correction for time-dependent inelastic processes before entrapment depths can be reliably inferred. The fracture nucleation diagrams and $V^{1/6}$ scaling laws derived here provide the quantitative framework to assess whether purely elastic interpretations are adequate.

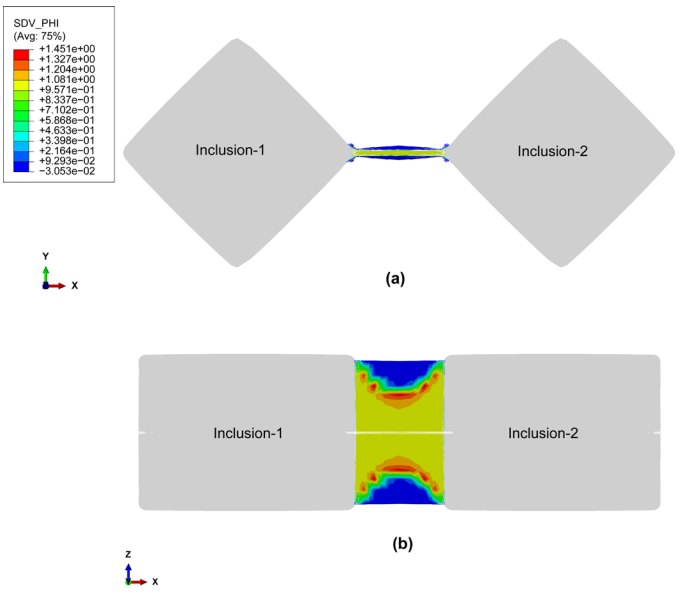

Figure 6 *Three-dimensional Phase-Field simulation of fracture coalescence between two interacting cuboidal inclusions. Top-down view (XY plane) showing symmetrical crack growth from each inclusion and their coalescence within the host. Side view (XZ plane) highlighting the through-thickness extent of the coalesced fracture. Yellow/red regions denote fully developed cracks (ϕ = 1). Although crack coalescence enhances local stress redistribution, the resulting pressure relaxation remains insufficient to reproduce natural residual pressures, highlighting the mechanical limits of fracture-only models.*

Beyond diamond systems, the computational framework is directly transferable to quartz-, coesite-, and zircon-in-garnet systems in metamorphic rocks, where the same mechanical configuration and analytical uncertainties apply. The framework therefore provides a general methodology for evaluating pressure-relaxation processes beyond the elastic approximation.

REFERENCES

Agrosì, G., Nestola, F., Tempesta, G., Bruno, M., Scandale, E., Harris, J.W. (2016) – X-ray topographic study of a diamond from Udachnaya: implications for the genetic nature of inclusions. Lithos, 248–251, 153–159.

Angel, R.J., Alvaro, M., Nestola, F., Mazzucchelli, M.L. (2015) – Diamond thermoelastic properties and implications for determining the pressure of formation of diamond-inclusion systems. Russ. Geol. Geophys., 56, 211–220.

Angel, R.J., Alvaro, M., Nestola, F. (2018) – 40 years of mineral elasticity: a critical review and a new parameterisation of equations of state for mantle olivines and diamond inclusions. Phys. Chem. Miner., 45, 95–113.

Angel, R.J., Alvaro, M., Nestola, F. (2022) – Crystallographic methods for non-destructive characterization of mineral inclusions in diamonds. Rev. Mineral. Geochem., 88, 257–305.

Bažant, Z.P. (2004) – Scaling theory for quasibrittle structural failure. Proc. Natl Acad. Sci., 101, 13400–13407.

Campomenosi, N., Angel, R.J., Alvaro, M., Mihailova, B. (2023) – Resetting of zircon inclusions in garnet: implications for elastic thermobarometry. Geology, 51, 23–27.

Field, J.E. & Pickles, C.S.J. (1996) – Strength, fracture and friction properties of diamond. Diamond Relat. Mater., 5, 625–634.

Kohn, M.J., Mazzucchelli, M.L., Alvaro, M. (2023) – Elastic thermobarometry. Annu. Rev. Earth Planet. Sci., 51, 331–366.

Miehe, C., Hofacker, M., Welschinger, F. (2010) – A phase field model for rate-independent crack propagation: robust algorithmic implementation based on operator splits. Comput. Methods Appl. Mech. Eng., 199, 2765–2778.

Moulas, E., Kostopoulos, D., Podladchikov, Y., Chatzitheodoridis, E., Schenker, F.L., Zingerman, K.M., Pomonis, P., Tajčmanová, L. (2020) – Calculating pressure with elastic geobarometry: a comparison of different elastic solutions with application to a calc-silicate gneiss from the Rhodope Metamorphic Province. Lithos, 378–379, 105803.

Nestola, F., Nimis, P., Ziberna, L., Longo, M., Marzoli, A., Harris, J.W., Manghnani, M.H., Periotto, B. (2011) – First crystal-structure determination of olivine in diamond: composition and implications for provenance in the Earth's mantle. Earth Planet. Sci. Lett., 305, 249–255.

Nestola, F., Korolev, N., Kopylova, M., Rotiroti, N., Pearson, D.G., Pamato, M.G., Alvaro, M., Peruzzo, L., Gurney, J.J., Moore, A.E., Davidson, J. (2018) – $CaSiO_3$ perovskite in diamond indicates the recycling of oceanic crust into the lower mantle. Nature, 555, 237–241.

Nimis, P., Alvaro, M., Nestola, F., Angel, R.J., Marquardt, K., Rustioni, G., Harris, J.W., Marone, F. (2016) – First evidence of hydrous silicic fluid films around solid inclusions in gem-quality diamonds. Lithos, 260, 384–389.

Pearson, D.G., Brenker, F.E., Nestola, F., McNeill, J., Nasdala, L., Hutchison, M.T., Matveev, S., Mather, K., Silversmit, G., Schmitz, S., Vekemans, B., Vincze, L. (2014) – Hydrous mantle transition zone indicated by ringwoodite included within diamond. Nature, 507, 221–224.

Puhan, B., Patton, A., Morganti, S., Rustioni, G., Reali, A., Alvaro, M. (2025) – Investigation of microscale brittle fracture opening in diamond with olivine inclusion using XFEM and cohesive zone modeling. Eng. Fract. Mech., 314, 110713.

Ritchie, R.O. (2011) – The conflicts between strength and toughness. Nat. Mater., 10, 817–822.

Rustioni, G., Alvaro, M., Nestola, F., Nimis, P., Harris, J.W. (2016) – Pressure release for host-inclusion systems: the interplay between brittle failure and fluid phase. EMC 2016, Book of Abstracts.

Weiss, Y., Czas, J., Navon, O. (2022) – Fluid inclusions in fibrous diamonds. Rev. Mineral. Geochem., 88, 475–532.

Whitney, D.L., Cooke, M.L., Du Frane, S.A. (2000) – Modeling of radial microcracks at corners of inclusions in garnet using fracture mechanics. J. Geophys. Res. Solid Earth, 105, 2843–2853.

Wu, J.-Y. (2017) – A unified phase-field theory for the mechanics of damage and quasi-brittle failure. J. Mech. Phys. Solids, 103, 72–99.

Zhong, X., Moulas, E., Tajčmanová, L. (2018) – Tiny timekeepers witnessing high-rate exhumation processes. Sci. Rep., 8, 2234.

Zhong, X., Wallis, D., Kingsbery, P., John, T. (2024) – The effect of aqueous fluid on viscous relaxation of garnet and modification of inclusion pressures after entrapment. Earth Planet. Sci. Lett., 636, 118713.